# Short-time photodissociation dynamics of A-band and B-band bromoiodomethane in solution: An examination of bond selective electronic excitation

Shi-Qing Man, Wai Ming Kwok, and David Lee Phillips[a)]
*Department of Chemistry, University of Hong Kong, Pokfulam Road, Hong Kong*

Alan E. Johnson
*Department of Chemistry, University of Rochester, Rochester, New York 14627*

(Received 26 March 1996; accepted 10 June 1996)

We have obtained resonance Raman spectra and absolute Raman cross section measurements at eight excitation wavelengths in the A-band and B-band absorptions of bromoiodomethane in cyclohexane solution. The resonance Raman intensities and absorption spectra were simulated using a simple model and time-dependent wave packet calculations. Normal mode vibrational descriptions were used with the results of the calculations to find the short-time photodissociation dynamics in terms of internal coordinates. The A-band short-time photodissociation dynamics indicate that the C–I bond becomes much longer, the C–Br bond becomes smaller, the I–C–Br angle becomes smaller, the H–C–Br angles become larger, the H–C–I angles become smaller, and the H–C–H angle becomes a bit smaller. The B-band short-time photodissociation dynamics indicate the C–Br bond becomes much longer, the C–I bond becomes slightly longer, the I–C–Br angle becomes smaller, the H–C–I angles become larger, the H–C–Br angles become smaller, and the H–C–H angle becomes slightly smaller. Both the A-band and B-band short-time photodissociation dynamics appear to be most consistent with an impulsive ''semi-rigid'' radical model qualitative description of the photodissociation with the $CH_2Br$ radical changing to a more planar structure in the A-band and the $CH_2I$ radical changing to a more planar structure in the B band. We have carried out a Gaussian deconvolution of the A-band and B-band absorption spectra of bromoiodomethane, as well as iodomethane and bromomethane. The absorption spectra, resonance Raman intensities, and short-time photodissociation dynamics suggest a moderate amount of coupling of the C–I and C–Br chromophores. © *1996 American Institute of Physics.* [S0021-9606(96)00735-0]

## I. INTRODUCTION

Many workers in the field of laser chemistry have been interested in investigating bond selective excitation and photochemistry.[1–56] Selective bond breaking has been demonstrated for electronic excitation to a directly dissociative state[1–4] and for electronic excitation to a part of the excited electronic state that is repulsive in the bond to be broken.[5–26] Control of selective bond breaking using several different methods such as coherent radiative control (CRC)[27–33] and optimal control theory (OCT)[34–41] have also been extensively studied theoretically and experimental demonstrations of controlling dissociative pathways have been reported.[42–45] These methods and simple electronic excitation of different bonds attempt to circumvent or compete with intramolecular vibrational energy redistribution that usually prevents selective bond breaking in thermal, overtone excitation, and infrared multiphoton excitation.[46–48] Recent experiments have also shown that bond selective chemistry can be achieved in bimolecular reactions.[49–56]

Several recent studies have examined solvent-induced symmetry breaking in molecules, with two equivalent dissociation channels such as diiodomethane[57,58] and triiodide ion.[59–62] The diiodomethane system allows comparison with the case of no solvent molecules nearby (i.e., gas phase photodissociation) and in this case the symmetry is not noticeably broken in the Franck–Condon region and the gas phase photodissociation initially proceeds mainly along the I–C–I symmetric stretch mode combined with spreading of the wave packet into the I–C–I antisymmetric mode and some I–C–I bending motion.[57,58,63,64] The gas phase A-state resonance Raman spectrum of diiodomethane shows no appreciable intensity in the I–C–I antisymmetric stretch fundamental or its combination bands with other modes.[58,63] However, when the photodissociation takes place in a solution phase environment there is a noticeable amount of symmetry breaking observed that leads to appreciable resonance Raman intensity in the I–C–I antisymmetric stretch fundamental (and its combination bands with I–C–I bend modes) in diiodomethane[57,58] and the I–I–I antisymmetric stretch fundamental in the triiodide ion.[59,60] It appears that when there is a large amount of symmetry breaking, the molecular system proceeds into the exit channel early and forms the photoproducts early in the solution phase.[58,60] The amount of symmetry breaking in both diiodomethane and triiodide ion appear to be very solvent dependent, and in the case of a triiodide ion there seems to be some correlation between the amount of symmetry breaking and the degree of vibrational coherence seen in the diiodide photofragment.[60–62]

In this paper we examine a prototypical example of se-

a)Author to whom correspondence should be addressed.

 0021-9606/96/105(14)/5842/16/$10.00 

lective bond breaking using electronic excitation of two different bonds in bromoiodomethane. We have carried out several resonance Raman experiments in order to examine the excited state dynamics in the Franck–Condon region at the vibrational mode specific level and attempt to learn more about the intramolecular interactions that enhance or inhibit bond selectivity. Bond selective photodissociation of bromoiodomethane upon excitation in the A-band and B-band absorptions has been observed in the gas phase.[1–3] Lee and Bersohn[1] carried out molecular beam experiments with broadband excitation of bromoiodomethane in the A band and found that 86% of the photodissociation reactions gave I atom photoproducts and 14% Br atom photoproducts. The anisotropy measurements from these experiments showed that the A-band photodissociation is fast relative to molecular rotation. Lee and Bersohn[1] also elucidated that the Br atoms observed in their experiments are from excitation to a different excited electronic state with a weaker transition. Butler *et al.*[2,3] later performed a more thorough molecular beam study on the photodissociation of bromoiodomethane. These later experiments[2,3] found that 210 nm excitation in the B-band absorption gave a definite preference for breaking the stronger C–Br bond with no scission of the C–I bond by itself. Butler *et al.*[2,3] also observed two minor photodissociation pathways leading to concerted elimination of electronically excited IBr and a three-body fragmentation forming $CH_2$+Br+I when bromoiodomethane is excited at 210 nm. These molecular beam experiments[1–3] have provided a large amount of information on the photodissociation dynamics of bromoiodomethane, but there has been very little vibrational mode-specific work reported that investigates the A-band and B-band photodissociation dynamics of bromoiodomethane. In this paper we report a vibrational mode-specific investigation of the A-band and B-band short-time photodissociation dynamics of bromoiodomethane in solution using resonance Raman spectroscopy.

The rest of the paper has the following structure. In Sec. II we describe the experimental methods and apparatus used to obtain the resonance Raman spectra and determine the absolute Raman cross sections of bromoiodomethane. In Sec. III we provide an overview of the calculations used to simulate the resonance Raman intensities and absorption spectra, as well as conversion of the short-time photodissociation dynamics into easy to visualize internal coordinate dynamics. In Sec. IV we show the results of the resonance Raman experiments and calculations. In Sec. IV we also provide a discussion of the results and the short-time photodissociation dynamics of bromoiodomethane. In Sec. V we give the conclusions of our resonance Raman investigation of bromoiodomethane.

## II. EXPERIMENT

Bromoiodomethane was synthesized using the methods previously reported by Miyano and Hashimoto.[65] The purity of the prepared bromoiodomethane was checked by NMR and UV/VIS absorption spectroscopies. The purity of the bromoiodomethane ranged from 94% to 98% and samples of about 0.14 M concentration were prepared for use in the resonance Raman experiments. The experimental methods and apparatus have been given elsewhere[57,58,66–68] so we will only give a brief description here. Various harmonics and hydrogen Raman shifted laser lines from a Nd:YAG laser provided the excitation frequencies for the resonance Raman experiments. The flowing liquid sample was excited by a laser beam ($\sim$50–100 $\mu$j) that was focused to approximately a 1 mm beam diameter. The Raman scattered light was collected by reflective optics and imaged through a depolarizer and entrance slit of a 0.5 m spectrometer (Acton). The spectrometer used a 1200 groove/mm grating blazed at 250 nm to disperse the Raman scattering onto a liquid nitrogen cooled CCD (Photometrics). About 30–40, 60 s scans are added up before being read out from the CCD to an interfaced PC compatible computer.

The known frequencies of cyclohexane were used to calibrate the Raman shifts observed in the experimental spectra. Using a backscattering geometry helps minimize the reabsorption of the Raman scattered light by a strongly absorbing sample, and the methods described in Refs. 69 and 70 were used to correct the spectra for the remaining reabsorption. The spectra were then solvent subtracted using an appropriately scaled solvent spectrum taken at the same spectral region as the bromoiodomethane spectrum (i.e., the monochromator was not moved between the bromoiodomethane scan and the solvent scan). The resonance Raman spectra were then corrected for the wavelength response of the detection system by using spectra taken of an intensity calibrated deuterium lamp. Sections of the resonance Raman spectra were fit to a baseline plus a sum of Lorentzian peaks. We observed no appreciable fluorescence underneath the A-band or B-band resonance Raman spectra of bromoiodomethane. We did observe some Rayleigh scattered light background in the low-frequency region and this was fit to a biexpotential baseline and subtracted to get the resonance Raman spectra baseline shown in Figs. 2 and 3 as well as the baseline for integrating the resonance Raman peaks.

Absolute resonance Raman cross sections of bromoiodomethane were measured relative to previously determined 802 $cm^{-1}$ and C–H stretch vibrational modes ($\sim$2900 $cm^{-1}$) of cyclohexane.[71,72] The bromoiodomethane/cyclohexane sample solution concentrations were found by taking absorption spectra (with a Perkin-Elmer 19 UV/VIS spectrometer) before and after the Raman experiments. Changes of less than 5% were observed in the bromoiodomethane/cyclohexane absorption spectra during the absolute Raman cross section measurements. The calculation of the absolute cross sections made use of the average concentration found from the initial and final concentrations from a series of experiments at each wavelength and an assumed depolarization ratio of 0.33. It appears that the electronic transitions are localized mostly on either the C–I bond for the A band or the C–Br bond for the B band. Because these two bonds have much different polarization directions, we would expect that the depolarization ratios could be very sensitive to any coupling or mixing of these transitions. We

are currently working on obtaining accurate depolarization ratio measurements for bromoiodomethane in cyclohexane (and several other solvents), and this will be reported in the future.[73] We measured the maximum molar extinction coefficients of bromoiodomethane in cyclohexane solution to be 900 $M^{-1}$ $cm^{-1}$ for the A band and 2870 $M-^{1}$ $cm^{-1}$ for the B band.

## III. THEORY AND CALCULATIONS

We have used a relatively simple model to calculate the absorption spectra and resonance Raman intensities associated with the A-band and B-band absorption transitions of bromoiodomethane in order to elucidate the major differences in the short-time photodissociation dynamics of the dominant transitions in the A and B bands. Our present calculations assume that the A-band and B-band absorptions are uncoupled, and thus we are ignoring any cross terms between the A-band and B-band transitions in order to keep things fairly simple. This model and calculations are not intended to be a complete description of the absorption and resonance Raman spectra, but will serve as a modest beginning to better understanding the vibrational-mode specific dynamics associated with the A-band and B-band transitions and as a reference with which more sophisticated calculations may be compared to assess the relative importance of processes or effects like coordinate dependence of the transition moment, possible Duschinsky rotation of normal coordinates, and others.

The absorption spectrum and resonance Raman cross sections were calculated for the A band and B bands separately using a time-dependent approach to resonance Raman scattering[74–79] with the absorption cross sections computed from the following equation:

$$\sigma_A(E_L)=\left(\frac{4\pi e^2 E_L M^2}{3n\hbar^2 c}\right)\sum_i P_i \,\mathrm{Re}\left[\int_0^\infty \langle i|i(t)\rangle \times \exp\left(\frac{i(E_L+\epsilon_i)t}{\hbar}\right)\exp[-g(t)]dt\right], \tag{1}$$

and the resonance Raman cross sections computed from this equation:

$$\sigma_R,(E_L,\omega_s)=\sum_i \sum_f P_i \sigma_{R,i\to f}(E_L)\,\delta(E_L+\epsilon_i-E_s-\epsilon_f),$$

with

$$\sigma_{R,i\to f}(E_L)=\left(\frac{8\pi e^4 {E_S}^3 E_L M^4}{9\hbar^6 c^4}\right)\left|\times\int_0^\infty \langle f|i(t)\rangle \exp\left(\frac{i(E_L+\epsilon_i)t}{\hbar}\right)\times\exp[-g(t)]dt\right|^2, \tag{2}$$

where $E_L$ is the incident photon energy, $E_S$ is the scattered photon energy, $n$ is the solvent index of refraction, $P_i$ is the initial Boltzmann population of the ground-state vibrational level $|i\rangle$, which has energy $\epsilon_i$ (the number of initial vibrational energy levels included in the Boltzmann sum was up to $v=4$ for $\nu_6$, $v=1$ for $\nu_5$, and $v=0$ for $\nu_4$), $\delta(E_L+\epsilon_i-E_S-\epsilon_f)$ is a delta function to add together cross sections with the same frequency, $M$ is the transition length evaluated at the equilibrium geometry, $|i(t)\rangle=e^{-iHt/\hbar}|i\rangle$ that is $|i(t)\rangle$ propagated on the excited state surface for a time $t$, $H$ is the excited state vibrational Hamiltonian, $f$ is the final state for the resonance Raman process, and $\epsilon_f$ is the energy of the ground-state vibrational level $|f\rangle$. The exp $[-g(t)]$ term in Eqs. (1) and (2) is a damping function that arises from population decay and/or solvent dephasing, and this was modeled as an exponential function. The lack of vibrational structure in the A-band and B-band gas, and solution phase absorption spectra suggests that the total electronic dephasing is dominated by photodissociation and/or solvent dephasing prior to the first vibrational recurrence. Furthermore, the lack of appreciable fluorescence in the resonance Raman spectra (at least up to 2500 $cm^{-1}$ Raman shift) suggests that the electronic dephasing is dominated by population decay due to photodissociation in the Franck–Condon region. The absorption cross sections and resonance Raman cross sections were computed from the preceding equations by the addition over a ground-state Boltzmann distribution of vibrational energy levels. We have used the Gaussian deconvolution of the experimental absorption spectrum to help guide the determination of the calculation parameters for fitting the absorption spectra.

We have assumed no coordinate dependence of the transition length (Condon approximation) and have used harmonic oscillators with their potential minima displaced by $\Delta$ in dimensionless normal coordinates (the displacements are defined with respect to the ground-state frequency) to approximate the ground- and excited state surfaces. The ground- and excited state harmonic oscillators could have either the same frequencies or different frequencies as appropriate. The bound harmonic oscillator model for the excited state just gives a convenient method to approximate the section of the excited state surface in the Franck–Condon region that decides the resonance Raman intensities and absorption spectrum, and does not imply that the excited state is actually bound. The analytic expressions from Mukamel and co-workers[79] were used to numerically calculate the time-dependent overlaps ($\langle i|i(t)\rangle$ and $\langle f|i(t)\rangle$) in Eqs. (1) and (2).

Typically, dimensionless normal coordinates are used to denote the harmonic potentials used in Eqs. (1) and (2). We convert the dimensionless normal coordinate motions into internal coordinate motions that are more readily comprehensible (i.e., bond length and bond angle changes) by using the following procedure. At a time $t$ after excitation to the excited electronic state, the center of the wave packet undergoing separable harmonic dynamics can be expressed in dimensionless normal coordinates by

$$q_\alpha(t)=\Delta_\alpha(1-\cos\,\omega_\alpha t), \tag{3}$$

where $\Delta_\alpha$ is the displacement along normal coordinate $\alpha$, the vibrational (excited state) frequency, $\omega_\alpha$, is in units of $fs^{-1}$, the time, $t$, is in units of fs, and we fix $q_\alpha=0$ for each mode

TABLE I. Bromoiodomethane ground-state normal modes.

| Mode | Experiment[a] frequency ($cm^{-1}$) | Calculated frequency ($cm^{-1}$) |
|---|---|---|
| $\nu_1$ | 2978 | 2978 |
| $\nu_2$ | 1374 | 1376 |
| $\nu_3$ | 1150 | 1150 |
| $\nu_4$ | 616 | 617 |
| $\nu_5$ | 517 | 512 |
| $\nu_6$ | 144 | 142 |
| $\nu_7$ | 3053 | 3053 |
| $\nu_8$ | 1065 | 1065 |
| $\nu_9$ | 754 | 754 |

[a]Frequencies are from Raman peaks observed in Refs. 80–82.

$\alpha$ at the ground electronic state equilibrium geometry. The internal coordinate changes from their ground-state equilibrium values at different times $t$ are then calculated from the dimensionless normal mode displacements, $q_\alpha(t)$, by the following formula:

$$s_i(t) = (h/2\pi c)^{1/2} \Sigma_\alpha A_{\alpha i} \varpi_\alpha{}^{-1/2} q_\alpha(t), \tag{4}$$

where $s_i$ are the changes in the internal coordinates (bond stretches, bends, torsions, and wags, as defined by Wilson, Decius, and Cross) from their ground electronic state equilibrium values, $A_{\alpha i}$ is the normal-mode coefficient $(\partial s_i/\partial Q_\alpha)$, $Q_\alpha$ is the ordinary dimensioned normal coordinate, and $\varpi_\alpha$ is the vibrational frequency in units of $cm^{-1}$. The normal-mode vectors of bromoiodomethane were calculated using an adapted version of the Snyder and Schachtschneider FG program (described in detail in Ref. 80) and previously published ground-state geometries and valence force fields[81] for bromoiodomethane. The force field gave a rms frequency error of 1.93 $cm^{-1}$ for the nine normal mode vibrations of bromoiodomethane and Table I shows a comparison of the calculated and experimental[81–83] frequencies. The complete force field, Cartesian coordinates, computed vibrational frequencies, and normal-mode coefficients are available as supplementary material.[84]

## IV. RESULTS AND DISCUSSION

### A. Absorption spectra

The absorption spectra of bromoiodomethane in cyclohexane solution, bromoiodomethane in the gas phase, bromomethane, and iodomethane are shown in Fig. 1. The excitation wavelengths for the resonance Raman experiments are displayed above the bromoiodomethane in the cyclohexane solution absorption spectrum. Both the gas and solution phase A- and B-band absorptions of bromoiodomethane have no vibrational structure, and this implies that the dissociation reactions take place faster than vibrational recurrences along any Franck–Condon active coordinate. The bromoiodomethane A-band absorption (maximum ~268 nm) has been assigned to a $n(I)\rightarrow\sigma^*$(C–I) transition and the B-band absorption (maximum ~213 nm) has been assigned to a $n$(Br)$\rightarrow\sigma^*$(C–Br) transition.[1] The A-band absorptions of bromomethane (maximum ~202 nm) and iodomethane

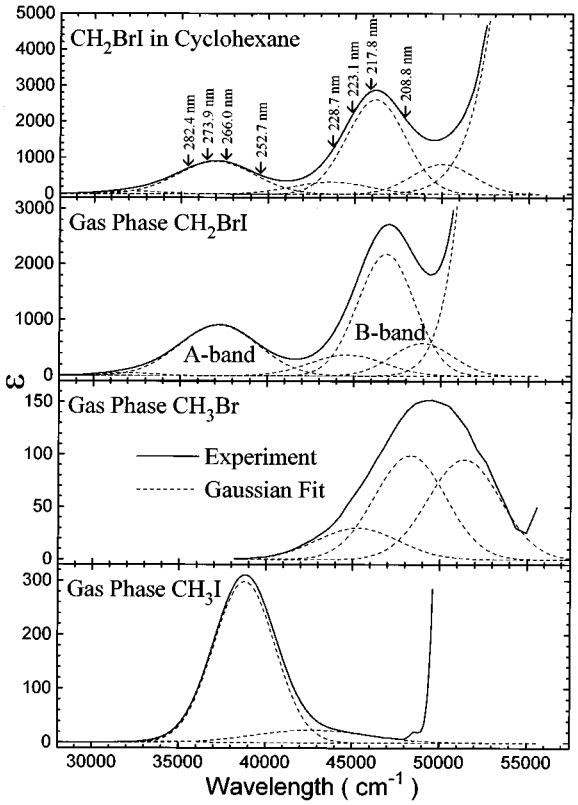


FIG. 1. The absorption spectra of bromoiodomethane in cyclohexane solution, gas phase bromoiodomethane, and gas phase iodomethane are displayed as solid lines. Gaussian curve fits to the absorption spectra are shown by dashed lines. The excitation wavelengths for the solution phase resonance Raman experiments are shown as numbers above the bromoiodomethane in cyclohexane solution absorption spectrum.

(maximum ~258 nm) also arise from $n$(X)$\rightarrow\sigma^*$(C–X) transitions. Examination of the position and the absorption extinction coefficients in Fig. 1 reveals that A and B bands of bromoiodomethane are redshifted and substantially more intense than the corresponding $n$(X)$\rightarrow\sigma^*$(C–X) transitions in bromomethane and iodomethane, which may be due to a degree of coupling of the C–I and C–Br chromophores in bromoiodomethane.

We have fit the absorption spectra displayed in Fig. 1 to a sum of Gaussian functions representing the N$\rightarrow$Q transitions that contribute to the $n$(X)$\rightarrow\sigma^*$(C–X) absorption bands. The iodomethane gas phase absorption was deconvoluted into three transitions for the A band ($^3Q_1$ around 34 446 $cm^{-1}$, $^3Q_0$ at 38 773 $cm^{-1}$, and $^1Q_1$ at 42 632 $cm^{-1}$), and this is in good agreement with the MCD measurements by Gedanken and Rowe.[85] Similarly we have also deconvoluted the gas phase bromomethane A-band absorption into three transitions ($^3Q_1$ around 45 260 $cm^{-1}$, $^3Q_0$ at 48 272 $cm^{-1}$, and $^1Q_1$ at 51 372 $cm^{-1}$), and this is in good agreement with the deconvolution given by Van Veen, Baller, and De Vries.[86] Comparing the deconvolutions of bromoiodomethane to the corresponding transitions in the iodomethane and bromomethane shows that the $^3Q_0$ transitions are greatly enhanced in intensity while the $^3Q_1$ and the $^1Q_1$ transitions do not appear to be enhanced as much in the A

and B bands of bromoiodomethane. The iodomethane $^3Q_1$ transition at 34 446 $cm^{-1}$ has a 2422 $cm^{-1}$ redshift in bromoiodomethane and the $^3Q_0$ transition at 38 773 $cm^{-1}$ has a 1572 $cm^{-1}$ redshift. The bromomethane $^3Q_1$ transition at 45 260 $cm^{-1}$ shifts to 44 616 $cm^{-1}$ (644 $cm^{-1}$ redshift), the $^3Q_0$ transition at 48 272 $cm^{-1}$ shifts to 46 829 $cm^{-1}$ (1443 $cm^{-1}$ redshift), and the $^1Q_1$ transition at 51 327 $cm^{-1}$ shifts to 48 911 $cm^{-1}$ (2416 $cm^{-1}$ redshift). The $^3Q_0$ and $^3Q_1$ transitions associated with the B band of bromoiodomethane are enhanced to a greater extent than the corresponding transitions of the A band relative to the same transitions in bromomethane and iodomethane.

The preceding observations about the absorption spectra of bromoiodomethane compared to iodomethane and bromomethane suggest that several factors influence the amount of oscillator strength and position of the N→Q transitions of the two chromophore bromoiodomethane compared to the single chromophore iodomethane and bromomethane. The smaller enhancement in the $^1Q_1$ transitions and the larger intensity enhancement of the $^3Q_1$ and $^3Q_0$ transitions imply that the large-intensity enhancement in bromoiodomethane has a multiplicity selection rule. The enhancement of the N→Q transitions is greater for the absorption band nearest the quasicontinuum above 50 000 $cm^{-1}$ in bromoiodomethane (i.e., the $^3Q_0$ transition intensity of the B band changes by about a factor of 22 times greater than the $^3Q_0$ transition of bromomethane, while the $^3Q_0$ transition intensity of the A band changes by about a factor of 3 times greater than the $^3Q_0$ transition of iodomethane). This suggests that part of the source of the intensity enhancement could come from mixing with states (having parallel character along either of the C–I and/or C–Br bonds) located within the broad quasicontinuum above 50 000 $cm^{-1}$. Robin[87] has noted that both energy and symmetry will determine the extent of mixing of valence $\sigma^*$ with the conjugate Rydberg sea of states.

However, some of the intensity enhancement may also be due to mixing of the electronic states associated with the A-band and B-band transitions of bromoiodomethane. In bromoiodomethane, the C–I and C–Br chromophore transitions are relatively near to one another in energy compared to chloroiodomethane, where the C–I and C–Cl chromophore transitions are more widely separated in energy. Although the C–I transitions in the A-band absorptions of bromoiodomethane and chloroiodomethane are located at almost the same energy (and presumably the C–I associated transitions located in the broad quasicontinuum above 50 000 $cm^{-1}$ are at very similar energies in both molecules), the intensity enhancement is a factor of 3 for bromoiodomethane but only about 1.4 for chloroiodomethane greater than the same transitions in iodomethane. This suggests that part of the intensity enhancement of the A band and/or the B band of bromoiodomethane may be due to appreciable mixing of the electronic states associated with the C–I and C–Br transitions. We also see some patterns in the resonance Raman spectra that may be indicative of this mixing and this will be discussed in more detail in Sec. IV D.

We should note a few caveats in our rather qualitative discussion of the bromoiodomethane absorption bands and comparison to the absorption spectra of bromomethane and iodomethane. Our Gaussian deconvolutions of the bromoiodomethane absorption spectra are mainly a convenient way to try and estimate the contributions of the $^3Q_1$, $^3Q_0$, and $^1Q_1$ transitions to the absorption bands and are probably not unambiguously determined. It would be more informative and reliable to have magnetic circular dichroism (MCD) measurements carried out on the A-band and B-band absorption of bromoiodomethane. Furthermore, it would be very helpful to have fairly accurate theoretical calculations on the electronic states associated with the A-band, B-band, and nearby Rydberg quasicontinuum absorptions of bromoiodomethane.

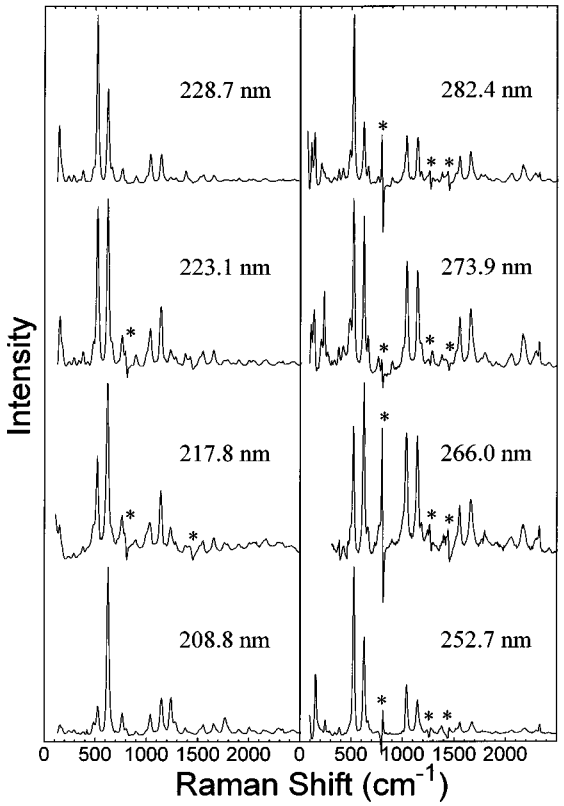


FIG. 2. Overview of the A-band and B-band resonance Raman spectra of bromoiodomethane in cyclohexane solution are shown. The displayed spectra have been intensity corrected and solvent subtracted. Solvent subtraction artifacts are labeled by asterisks (*).

### B. Resonance Raman spectra

Figure 2 shows an overview of the A-band and B-band resonance Raman spectra of bromoiodomethane in cyclohexane solution. Figure 3 displays a larger view of the 208.8 nm and 217.8 nm B band and 252.7 and 266.0 nm A-band resonance Raman spectra, with tentative spectral assignments shown for some of the larger Raman peaks. The spectra presented in Figs. 2 and 3 have been intensity corrected and solvent subtracted. Solvent subtraction of the very strong cyclohexane C–H stretch peaks leaves the spectra very noisy between 2800 and 3100 $cm^{-1}$ and this part of the spectra are

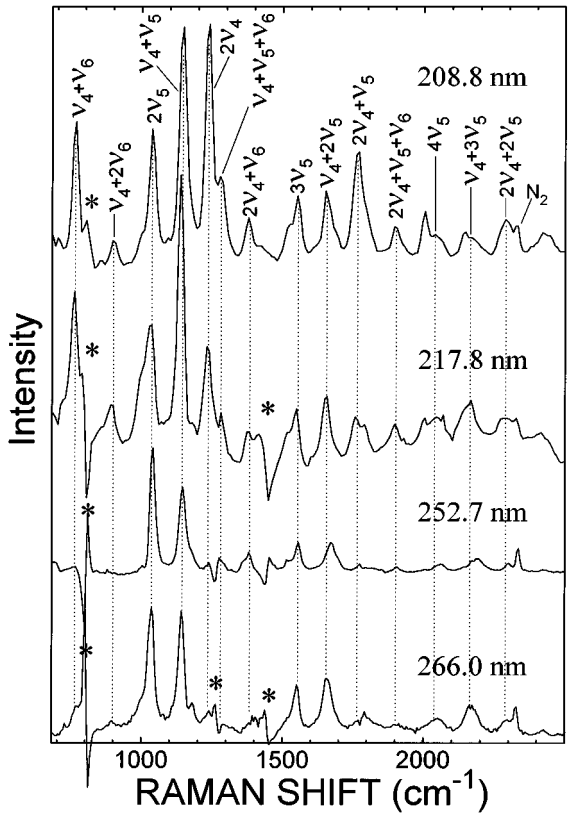


FIG. 3. An expanded view of the B-band 208.8 and 217.8 nm resonance Raman spectra and the A-band 252.7 and 266.0 nm resonance Raman spectra. The spectra have been intensity corrected and solvent subtracted with solvent subtraction artifacts marked by asterisks (*). Several larger Raman peaks in the spectra are labeled with tentative assignments.

not shown. The larger Raman peaks labeled in Fig. 3 have been tentatively assigned based on previously published nonresonant Raman and infrared spectra.[81–83] Almost all of the resonance Raman peaks in Figs. 2 and 3 can be assigned to fundamentals, overtones, and combination bands of $\nu_4$ (the nominal C–Br stretch), $\nu_5$ (the nominal C–I stretch), and $\nu_6$ (the nominal I–C–Br bend). Table II gives the Raman shifts and relative intensities of the bromoiodomethane peaks shown in the resonance Raman spectra of Figs. 2 and 3. Because fundamental Raman peaks are often susceptible to interference effects from contributions to their intensities from other electronic states, we have scaled our resonance Raman intensities to the first overtone of the nominal C–I stretch peak ($2\nu_5$). Our scaling standard of $2\nu_5$ also provides us a convenient method of comparing the differences in the A-band and B-band excited states relative to the nominal C–I stretch motion in each band. The A-band resonance Raman spectra of iodomethane and higher iodoalkanes have their fundamental intensities affected by preresonant contributions from higher lying excited electronic states,[88–90] and it is very likely that the fundamental intensities of the bromoiodomethane could have similar contributions to their fundamental intensities from some of the excited states in the very strong and broad quasicontinuum of states below 200 nm. Thus, we will concentrate our attention to the overtones and combination bands that are seen in our resonance Raman spectra.

Inspection of Figs. 2 and 3 and Table II shows that there are very noticeable differences between the A-band and B-band resonance Raman spectra. The B-band resonance Raman spectra generally have a larger amount of intensity in the overtone ($2\nu_4$) of the nominal C–Br stretch mode, the combination bands of the nominal C–Br stretch fundamental, and overtone with fundamentals and overtones of the nominal C–I stretch and Br–C–I bending modes ($\nu_4+\nu_5$, $\nu_4+\nu_6$, $\nu_4+2\nu_6$, $\nu_4-\nu_6$, $2\nu_4+\nu_6$, $2\nu_4+\nu_5$, $2\nu_4+2\nu_5$, $\nu_4+\nu_5+\nu_6$, $\nu_4+\nu_5-\nu_6$, and $2\nu_4+\nu_5+\nu_6$) than the A-band resonance Raman spectra. Qualitatively this observation would suggest that photoexcitation in the B-band absorption results in more motion along the nominal C–Br and nominal I–C–Br bending vibrational modes than photoexcitation in the A-band absorption. This is also consistent with the results of the molecular beam experiments that show A-band photoexcitation leads predominantly to C–I bond cleavage and B-band photoexcitation leads predominantly to C–Br bond cleavage. Both the A-band and B-band resonance Raman spectra have considerable intensity in overtones and/or combination bands of $\nu_4$ (the nominal C–Br stretch), $\nu_5$ (the nominal C–I stretch), and $\nu_6$ (the nominal I–C–Br bend). This strongly suggests that the photodissociation reactions occurring in the A band and B bands have multidimensional character and/or mixing of the internal coordinates in the ground state normal modes. In order to determine the importance of these two effects and elucidate the internal coordinate changes that take place during the short-time photodissociation dynamics, we need to carry out a quantitative resonance Raman intensity analysis that also makes use of the normal mode descriptions of the Franck–Condon active modes.

### C. Simulations of absorption and resonance Raman spectra and photodissociation dynamics

The A-band and B-band absorption spectra and resonance Raman intensities of bromoiodomethane were simulated using the model described in Sec. III and the parameters given in Table III in Eqs. (1) and (2). The excitation wavelengths near the center of the A band and B bands were given more weight when determining the normal mode-displacement parameters that give the best fit to the resonance Raman overtone and combination band intensities. Since the $^3Q_0$ transitions most likely dominates both the A-band and B-band absorption spectra, and we are using a relatively simple single state model to simulate each band separately, we have modeled the dominant Gaussian curve from the deconvolution of the A-band and B-band absorption spectra of bromoiodomethane. Population decay due to direct photodissociation causes (at least for lower final vibrational states) the $\langle i|i(t)\rangle$ and $\langle f|i(t)\rangle$ overlaps to decrease very rapidly as the wave packet leaves the Franck–Condon region. In addition to the population decay due to direct photodissociation, we used a homogeneous HWHM linewidth of

TABLE II. Resonance Raman intensities of bromoiodomethane in cyclohexane solution.

A. A-band excitation wavelengths

| Peak | Raman shift ($cm^{-1}$)[a] | 252.7 nm intensity[b] | 266.0 nm intensity[b] | 273.9 nm intensity[b] | 282.4 nm intensity[b] |
|---|---|---|---|---|---|
| $\nu_5$ | 521 | 298 | 87 | 132 | 365 |
| $2\nu_5$ | 1034 | 100 | 100 | 100 | 100 |
| | | $(1.10\times10^{-10})$[d] | $(3.45\times10^{-10})$[d] | $(1.76\times10^{-10})$[d] | $(6.27\times10^{-11})$[d] |
| $3\nu_5$ | 1550 | 23 | 35 | 48 | 85 |
| $4\nu_5$ | 2050 | 12 | 26 | 35 | 87 |
| $\nu_4$ | 621 | 191 | 127 | 129 | 177 |
| $2\nu_4$ | 1236 | 16 | 15 | 7 | 12 |
| $\nu_6$ | 151 | 115 | c | c | 141 |
| $2\nu_6$ | 289 | 2 | c | c | 3 |
| $\nu_4+\nu_5$ | 1140 | 79 | 96 | 102 | 138 |
| $\nu_4+2\nu_5$ | 1657 | 43 | 69 | 84 | 124 |
| $\nu_4+3\nu_5$ | 2163 | 30 | 53 | 72 | 116 |
| $\nu_4+\nu_6$ | 764 | <2 | 20 | 18 | 17 |
| $\nu_4+2\nu_6$ | 893 | <2 | 6 | 10 | 18 |
| $\nu_4-\nu_6$ | 487 | 31 | 39 | 58 | 82 |
| $\nu_5+\nu_6$ | 662 | 14 | 20 | 27 | 29 |
| $\nu_5-\nu_6$ | 378 | 16 | 11 | <2 | 20 |
| $2\nu_5+\nu_6$ | 1182 | 12 | 11 | 17 | 14 |
| $2\nu_4+\nu_6$ | 1381 | 16 | <2 | 9 | 29 |
| $2\nu_4+\nu_5$ | 1758 | <2 | 3 | 3 | 17 |
| $2\nu_4+2\nu_5$ | 2291 | 6 | 14 | 31 | 59 |
| $\nu_4+\nu_5+\nu_6$ | 1283 | 18 | 9 | 13 | 40 |
| $\nu_4+\nu_5-\nu_6$ | 1002 | 1 | 38 | 23 | 26 |
| $\nu_4+2\nu_5+\nu_6$ | 1793 | 3 | 18 | 21 | 31 |
| $\nu_4+2\nu_5-\nu_6$ | 1523 | 8 | 17 | 17 | 31 |
| $2\nu_4+\nu_5+\nu_6$ | 1897 | 3 | 8 | 15 | 23 |

B. B-band excitation wavelengths

| Peak | Raman shift ($cm^{-1}$)[a] | 208.8 nm intensity[b] | 217.8 nm intensity[b] | 223.1 nm intensity[b] | 228.7 nm intensity[b] |
|---|---|---|---|---|---|
| $\nu_5$ | 521 | 133 | 295 | 389 | 477 |
| $2\nu_5$ | 1034 | 100 | 100 | 100 | 100 |
| | | $(2.52\times10^{-9})$[d] | $(2.62\times10^{-9})$[d] | $(1.03\times10^{-9})$[d] | $(3.41\times10^{-10})$[d] |
| $3\nu_5$ | 1550 | 48 | 47 | 48 | 21 |
| $4\nu_5$ | 2050 | 30 | 35 | 27 | 12 |
| $\nu_4$ | 621 | 814 | 648 | 402 | 288 |
| $2\nu_4$ | 1236 | 207 | 98 | 42 | 20 |
| $\nu_6$ | 151 | 73 | 40 | 111 | 185 |
| $2\nu_6$ | 289 | 20 | 15 | 17 | 19 |
| $\nu_4+\nu_5$ | 1140 | 209 | 207 | 152 | 97 |
| $\nu_4+2\nu_5$ | 1657 | 71 | 70 | 58 | 26 |
| $\nu_4+3\nu_5$ | 2163 | 22 | 58 | 36 | 11 |
| $\nu_4+\nu_6$ | 764 | 112 | 106 | 53 | 48 |
| $\nu_4+2\nu_6$ | 893 | 23 | 38 | 33 | 26 |
| $\nu_4-\nu_6$ | 487 | 66 | 54 | 52 | 43 |
| $\nu_5+\nu_6$ | 662 | 17 | 46 | 41 | 35 |
| $\nu_5-\nu_6$ | 378 | 13 | 21 | 29 | 31 |
| $2\nu_5+\nu_6$ | 1182 | <2 | <2 | 14 | <2 |
| $2\nu_4+\nu_6$ | 1381 | 39 | 50 | 36 | 41 |
| $2\nu_4+\nu_5$ | 1758 | 112 | 44 | 13 | 6 |
| $2\nu_4+2\nu_5$ | 2291 | 57 | 44 | 15 | 7 |
| $\nu_4+\nu_5+\nu_6$ | 1283 | 66 | 41 | 16 | 10 |
| $\nu_4+\nu_5-\nu_6$ | 1002 | 19 | 62 | 42 | 21 |
| $\nu_4+2\nu_5+\nu_6$ | 1793 | 29 | 25 | 20 | 6 |
| $\nu_4+2\nu_5-\nu_6$ | 1523 | 24 | 30 | 33 | 18 |
| $2\nu_4+\nu_5+\nu_6$ | 1897 | 27 | 31 | 19 | 11 |

[a]Estimated uncertainties are about 4 $cm^{-1}$ for the Raman shifts.
[b]Relative intensities are based on integrated areas of the peaks. Estimated uncertainties are about 15% for intensities greater than 50 and 25% for intensities below 50.
[c]Rayleigh scattering from laser line was too large to observe these peaks in the 266 and 273.9 nm resonance Raman spectra.
[d]Absolute Raman cross section for $2\nu_5$ in $Å^2$/molecule.

TABLE III. Parameters for calculation of resonance Raman intensities and absorption spectra of A-band and B-band bromoiodomethane.

| A-Band parameters. Transition length, $M=0.287$ Å; $E_0=27\,200$ cm$^{-1}$; HWHM of damping function, $\Gamma=50$ cm$^{-1}$. | | | |
|---|---|---|---|
| Vibrational mode | Ground-state vibrational frequency (cm$^{-1}$) | Excited state vibrational frequency (cm$^{-1}$) | $\|\Delta\|$ |
| $\nu_4$ | 621 cm$^{-1}$ | 621 cm$^{-1}$ | 2.65 |
| $\nu_5$ | 521 cm$^{-1}$ | 521 cm$^{-1}$ | 4.8 |
| $\nu_6$ | 151 cm$^{-1}$ | 151 cm$^{-1}$ | 4.5 |
| **B-Band parameters. Transition length, $M=0.38$ Å; $E_0=41\,100$ cm$^{-1}$; HWHM of damping function, $\Gamma=50$ cm$^{-1}$.** | | | |
| Vibrational mode | Ground-state vibrational frequency (cm$^{-1}$) | Excited state vibrational frequency (cm$^{-1}$) | $\|\Delta\|$ |
| $\nu_4$ | 621 cm$^{-1}$ | 621 cm$^{-1}$ | 2.5 |
| $\nu_5$ | 521 cm$^{-1}$ | 521 cm$^{-1}$ | 3.0 |
| $\nu_6$ | 151 cm$^{-1}$ | 151 cm$^{-1}$ | 3.6 |

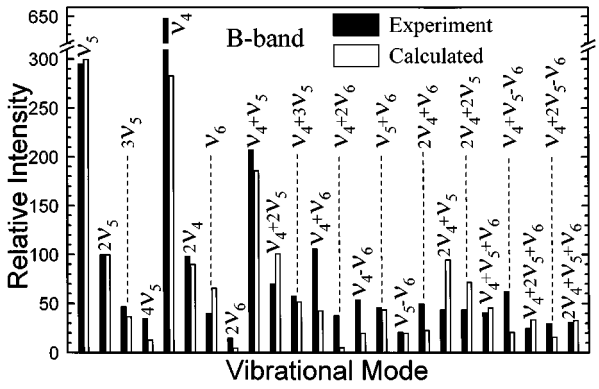


FIG. 4. Comparison of experimental (solid bar) and calculated (open bar) resonance Raman intensities for the B-band 217.8 nm resonance Raman spectrum of bromoiodomethane in cyclohexane solution. The calculated resonance Raman intensities were computed using the B-band parameters given in Table III in Eqs. (1) and (2) and the model described in Sec. III.

50 cm$^{-1}$ that corresponds to an excited state lifetime of about 55 fs for both the A and B bands. This extra damping of the overlaps in order to better fit the absolute Raman cross sections may be due to radiationless decay to another surface or solvent dephasing interactions. Although 55 fs is close to the vibrational recurrence time of the 621 cm$^{-1}$ mode, this recurrence does not contribute significantly to the calculated Raman intensities because of the multidimensionality of the photodissociation where the other two vibrationally active modes have different recurrence times. The calculated relative Raman intensities have little dependence on the value of the homogeneous linewidth used to mimic the radiationless decay to another surface and/or solvent dephasing. However, there is a moderate dependence of the absolute Raman cross section on the homogeneous and we fit the $2\nu_5$ absolute Raman cross sections of the 266.0 nm resonance Raman spectrum in the A band and the 217.8 nm resonance Raman spectrum in the B band. This procedure is very similar to one used to find population decay time estimates from the lowest allowed singlet states of cis-hexatriene (20 fs)[91] and trans-hexatriene (40 fs)[92,93] from fitting the absolute Raman cross sections by varying the homogeneous linewidth. We note that the photodissociation times of other iodoalkanes such as iodomethane and diiodomethane are in the range of 50–100 fs.[63,64,94–97] Several resonance Raman studies on the A band of iodomethane showed that at least for the first few overtones and combination bands, the resonance Raman intensities (and depolarization ratios) near the center of the absorption band are not noticeably affected by the known $^3Q_0 \rightarrow {}^1Q_1$ curve crossing.[89,90,98,99] However, for higher overtones there is some disagreement.[98,99] It also seems unlikely that any radiationless decay mechanism would give very similar rates for both the A band and B band of bromoiodomethane in light of the rich photochemistry of the B-band relative to the A-band photodissociation. Thus, we think that the additional damping is most likely due to solvent dephasing that occurs on a similar time scale as the photodissociation.

The calculated B-band absorption curve is broad, featureless, and fits the $^3Q_0$ Gaussian curve in Fig. 5 well. There is reasonable agreement between the 217.8 nm calculated and experimental resonance Raman intensities displayed in Fig. 4. There is also good agreement between the calculated and experimental absolute resonance Raman cross section for the $2\nu_5$ peak (calc.$=2.40\times10^{-9}$ Å$^2$/molecule compared to expt.$=2.62\times10^{-9}$ Å$^2$/molecule). There is noticeably worse agreement between the calculated and experimental relative resonance Raman intensities as well as absolute resonance Raman cross sections for the 208.8 and 228.7 nm resonance Raman spectra. This is not unexpected since the $^3Q_0$ transition seems to be less dominant at these wavelengths with the $^3Q_1$ transition contributing more at 228.7 nm and the $^1Q_1$ transition contributing more at 208.8 nm.

There is reasonable agreement between the A-band calculated and experimental relative resonance Raman intensities shown in Fig. 6 as well as good agreement between the $2\nu_5$ calculated and experimental absolute resonance Raman cross sections for 266.0 nm, as shown in Table IV (calc.$=3.50\times10^{-10}$ Å$^2$/molecule compared to expt.$=3.45$

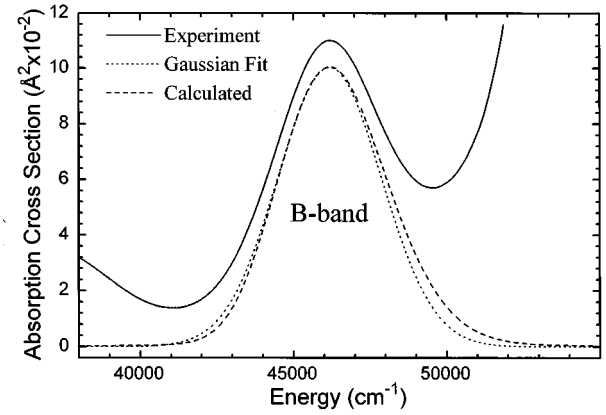


FIG. 5. Comparison of experimental (solid line), Gaussian fit (dotted line), and calculated (dashed line) B-band absorption spectra. The calculated absorption spectrum was determined using the B-band parameters in Table III in Eqs. (1) and (2) and the model described in Sec. III.

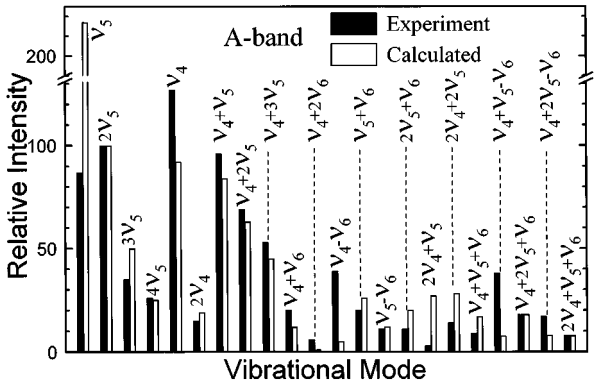


FIG. 6. Comparison of experimental (solid bar) and calculated (open bar) resonance Raman intensities for the A-band 266.0 nm resonance Raman spectrum of bromoiodomethane in cyclohexane solution. The calculated Raman intensities were found by using the A-band parameters of Table III in Eqs. (1) and (2) and the model described in Sec. III.

$\times 10^{-10}$ Å$^2$/molecule). Examination of Table IV shows that the A-band relative resonance Raman calculated and experimental intensities appear to have better overall agreement than the B band. This may just be a result of the A-band absorption having a higher degree of $^3Q_0$ transition character than the B-band absorption. The calculated $2\nu_5$ absolute Raman cross sections are a bit too large compared to the A-band 252.7, 273.9, and 282.4 nm experimental values (see Table IV). We can achieve a somewhat better fit to the A-band resonance Raman absolute cross sections using parameters that give a noticeably sharper calculated absorption, but this would not be in good agreement with the Gaussian deconvolution of the A-band absorption. If we had a more accurate description of the relative contributions of these transitions to the absorption bands based on magnetic circular dichroism (MCD) measurements and/or other experimental data, we would probably simultaneously model the dominant $^3Q_0$ transition and the wavelength dependence of the absolute resonance Raman cross sections better than the present simulations.

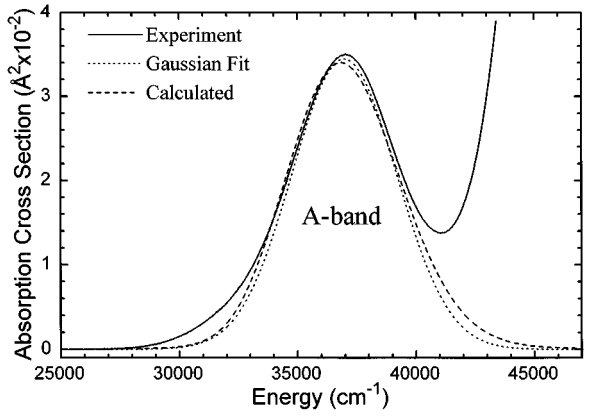


FIG. 7. Comparison of experimental (solid line), Gaussian fit (dotted line), and calculated (dashed line) A-band absorption spectra. The computed absorption spectrum was found by using the A-band parameters of Table III in Eqs. (1) and (2) and the model given in Sec. III.

While our model and simulations are not the most accurate description of the absorption spectrum and resonance Raman intensities of the A band and B bands of bromoiodomethane in cyclohexane solution, they do serve as a reasonable approximation to elucidate the major differences and similarities of the A-band and B-band $^3Q_0$ electronic excited states and dynamics in the Franck–Condon region in a quantitative manner. Our model parameters used to simulate the A-band and B-band absorption spectra and resonance Raman intensities are listed in Table III, with the normal mode displacements, $\Delta$, given in dimensionless normal coordinates. In order to easily visualize the short-time photodissociation dynamics of the A and B bands of bromoiodomethane, we have used the results of normal coordinate calculations in conjunction with Eqs. (4) and (5) to find the internal coordinate displacements at 15 fs after photoexcitation. We have chosen 15 fs since at that time the nuclei have not moved very far from the Franck–Condon region and 15 fs is relatively short with respect to the vibrational recurrence times of the Franck–Condon active normal modes. Since our resonance Raman intensity analysis only provides us the magnitude of the normal coordinate displacements, we need some method to find the signs of the normal mode displacements. The problem of picking the signs of the normal coordinate displacements has been discussed in detail in several recent reviews on resonance Raman intensity analysis.[70,100] For our present work on bromoiodomethane, we shall use some chemical intuition to help eliminate several of the possible sign combinations of the normal mode displacement parameters.

The normal modes of the nominal C–I stretch ($\nu_5$) and the nominal C–Br stretch ($\nu_4$) have large components of both the C–I stretch and C–Br stretch internal coordinates. The nominal C–I stretch ($\nu_5$) normal mode has a symmetric I–C–Br stretch character and the nominal C–Br stretch ($\nu_4$) normal mode has an antisymmetric I–C–Br stretch character. This information combined with the results of the molecular beam experiments that indicate excitation in the A-band absorption leads predominantly to direct C–I bond cleavage and excitation in the B-band absorption leads mostly to direct C–Br bond cleavage can be used to choose the most likely sign combinations of the normal coordinate displacements. Photoexcitation within the A-band absorption apparently leads to direct C–I bond breaking, and this implies that the C–I bond is lengthening during the initial dissociation. The sign of $\Delta_5$ should be positive in order to have the C–I bond lengthen during the initial photodissociation. A positive sign for $\Delta_4$ would make the C–Br bond lengthen much faster than the C–I bond (this is more consistent with C–Br bond cleavage), which is not consistent with the predominant direct C–I bond breaking associated with A-band photoexcitation. Thus, the most likely sign combinations for the A band are positive for $\Delta_5$, negative for $\Delta_4$, and $\Delta_6$ can be either negative or positive. Using these possible sign combinations for the normal mode displacements, we used Eqs. (3) and (4) to find the internal coordinate displacements 15 fs

TABLE IV. Comparison of experimental and calculated resonance Raman intensities of bromoiodomethane in cyclohexane solution.

A. A-band excitation wavelengths

| Peak | Raman shift ($cm^{-1}$)[a] | 252.7 nm | | 266.0 nm | | 273.9 nm | | 282.4 nm | |
|---|---|---|---|---|---|---|---|---|---|
| | | expt. | calc. | expt. | calc. | expt. | calc. | expt. | calc. |
| $\nu_5$ | 521 | 298 | 223 | 87 | 217 | 132 | 217 | 365 | 220 |
| $2\nu_5$ | 1034 | 100 | 100 | 100 | 100 | 100 | 100 | 100 | 100 |
| Expt.= | | $(1.10\times10^{-10})$[c] | | $(3.45\times10^{-10})$[c] | | $(1.76\times10^{-10})$[c] | | $(6.27\times10^{-11})$[c] | |
| Calc.= | | $(2.36\times10^{-10})$[c] | | $(3.50\times10^{-10})$[c] | | $(3.36\times10^{-10})$[c] | | $(2.63\times10^{-10})$[c] | |
| $3\nu_5$ | 1550 | 23 | 50 | 35 | 50 | 48 | 50 | 85 | 50 |
| $4\nu_5$ | 2050 | 12 | 24 | 26 | 25 | 35 | 26 | 87 | 25 |
| $\nu_4$ | 621 | 191 | 96 | 127 | 92 | 129 | 92 | 177 | 93 |
| $2\nu_4$ | 1236 | 16 | 19 | 15 | 19 | 7 | 19 | 12 | 19 |
| $\nu_6$ | 151 | 115 | 27 | [b] | 29 | [b] | 30 | 141 | 31 |
| $2\nu_6$ | 289 | 2 | 1 | [b] | 2 | [b] | 2 | 3 | 2 |
| $\nu_4+\nu_5$ | 1140 | 79 | 85 | 96 | 84 | 102 | 84 | 138 | 83 |
| $\nu_4+2\nu_5$ | 1657 | 43 | 64 | 69 | 63 | 84 | 63 | 124 | 62 |
| $\nu_4+3\nu_5$ | 2163 | 30 | 45 | 53 | 45 | 72 | 44 | 116 | 43 |
| $\nu_4+\nu_6$ | 764 | <2 | 11 | 20 | 12 | 18 | 12 | 17 | 12 |
| $\nu_4+2\nu_6$ | 893 | <2 | <1 | 6 | 1 | 10 | 1 | 18 | 1 |
| $\nu_4-\nu_6$ | 487 | 31 | 4 | 39 | 5 | 58 | 5 | 82 | 6 |
| $\nu_5+\nu_6$ | 662 | 14 | 24 | 20 | 26 | 27 | 27 | 29 | 28 |
| $\nu_5-\nu_6$ | 378 | 16 | 10 | 11 | 12 | <2 | 13 | 20 | 14 |
| $2\nu_5+\nu_6$ | 1182 | 12 | 18 | 11 | 20 | 17 | 20 | 14 | 21 |
| $2\nu_4+\nu_6$ | 1381 | 16 | 4 | <2 | 4 | 9 | 4 | 29 | 4 |
| $2\nu_4+\nu_5$ | 1758 | <2 | 28 | 3 | 27 | 3 | 27 | 17 | 26 |
| $2\nu_4+2\nu_5$ | 2291 | 6 | 29 | 14 | 28 | 31 | 28 | 59 | 27 |
| $\nu_4+\nu_5+\nu_6$ | 1283 | 18 | 16 | 9 | 17 | 13 | 18 | 40 | 18 |
| $\nu_4+\nu_5-\nu_6$ | 1002 | 1 | 6 | 38 | 8 | 23 | 8 | 26 | 9 |
| $\nu_4+2\nu_5+\nu_6$ | 1793 | 3 | 16 | 18 | 18 | 21 | 18 | 31 | 19 |
| $\nu_4+2\nu_5-\nu_6$ | 1523 | 8 | 7 | 17 | 8 | 17 | 9 | 31 | 10 |
| $2\nu_4+\nu_5+\nu_6$ | 1897 | 3 | 7 | 8 | 8 | 15 | 8 | 23 | 8 |

B. B-band excitation wavelengths

| Peak | Raman shift[a] ($cm^{-1}$) | 200.8 nm | | 217.8 nm | | 223.1 nm | | 228.7 nm | |
|---|---|---|---|---|---|---|---|---|---|
| | | expt. | calc. | expt. | calc. | expt. | calc. | expt. | calc. |
| $\nu_5$ | 521 | 133 | 307 | 295 | 300 | 389 | 305 | 477 | 323 |
| $2\nu_5$ | 1034 | 100 | 100 | 100 | 100 | 100 | 100 | 100 | 100 |
| Expt. | | $(2.52\times10^{-9})$[c] | | $(2.62\times10^{-9})$[c] | | $(1.03\times10^{-9})$[c] | | $(3.41\times10^{-10})$[c] | |
| Calc. | | $(1.74\times10^{-9})$[c] | | $(2.40\times10^{-9})$[c] | | $(1.72\times10^{-9})$[c] | | $(7.90\times10^{-10})$[c] | |
| $3\nu_5$ | 1550 | 48 | 36 | 47 | 37 | 48 | 37 | 21 | 36 |
| $4\nu_5$ | 2050 | 30 | 12 | 35 | 13 | 27 | 14 | 12 | 13 |
| $\nu_4$ | 621 | 814 | 297 | 648 | 283 | 402 | 284 | 288 | 298 |
| $2\nu_4$ | 1236 | 207 | 94 | 98 | 90 | 42 | 88 | 20 | 86 |
| $\nu_6$ | 151 | 73 | 60 | 40 | 66 | 111 | 72 | 185 | 81 |
| $2\nu_6$ | 289 | 20 | 4 | 15 | 5 | 17 | 6 | 19 | 8 |
| $\nu_4+\nu_5$ | 1140 | 209 | 192 | 207 | 186 | 152 | 182 | 97 | 179 |
| $\nu_4+2\nu_5$ | 1657 | 71 | 104 | 70 | 101 | 58 | 98 | 26 | 93 |
| $\nu_4+3\nu_5$ | 2163 | 22 | 53 | 58 | 52 | 36 | 50 | 11 | 47 |
| $\nu_4+\nu_6$ | 764 | 112 | 39 | 106 | 43 | 53 | 45 | 48 | 48 |
| $\nu_4+2\nu_6$ | 893 | 23 | 4 | 38 | 6 | 33 | 6 | 26 | 7 |
| $\nu_4-\nu_6$ | 487 | 66 | 16 | 54 | 20 | 52 | 21 | 43 | 23 |
| $\nu_5+\nu_6$ | 662 | 17 | 39 | 46 | 44 | 41 | 48 | 35 | 51 |
| $\nu_5-\nu_6$ | 378 | 13 | 16 | 21 | 20 | 29 | 24 | 31 | 26 |
| $2\nu_5+\nu_6$ | 1182 | <2 | 21 | <2 | 24 | 14 | 26 | <2 | 28 |
| $2\nu_4+\nu_6$ | 1381 | 39 | 21 | 50 | 23 | 36 | 24 | 41 | 24 |
| $2\nu_4+\nu_5$ | 1758 | 112 | 100 | 44 | 95 | 13 | 91 | 6 | 86 |
| $2\nu_4+2\nu_5$ | 2291 | 57 | 76 | 44 | 72 | 15 | 68 | 7 | 63 |
| $\nu_4+\nu_5+\nu_6$ | 1283 | 66 | 41 | 41 | 46 | 16 | 47 | 10 | 48 |
| $\nu_4+\nu_5-\nu_6$ | 1002 | 19 | 17 | 62 | 21 | 42 | 24 | 21 | 25 |
| $\nu_4+2\nu_5+\nu_6$ | 1793 | 29 | 31 | 25 | 34 | 20 | 35 | 6 | 35 |
| $\nu_4+2\nu_5-\nu_6$ | 1523 | 24 | 13 | 30 | 16 | 33 | 18 | 18 | 19 |
| $2\nu_4+\nu_5+\nu_6$ | 1897 | 27 | 30 | 31 | 33 | 19 | 33 | 11 | 33 |

[a]Estimated uncertainties are about 4 $cm^{-1}$ for the Raman shifts.
[b]Rayleigh scattering from laser line was too large to observe these peaks in the 266 and 273.9 nm resonance Raman spectra.
[c]Absolute Roman cross section for $2\nu_5$ in $Å^2$/molecule.

TABLE V. Most probable internal coordinate displacements of bromoiodomethane in cyclohexane solution at $t=15$ fs, assuming the C–I bond lengthens in the A band and the C–Br bond lengthens in the B band.

| | Range of displacements at $t=15$ fs[a] | |
|---|---|---|
| A band<br>Internal coordinate | $\Delta_4=-2.65$<br>$\Delta_5=+4.8$, $\Delta_6=+4.5$ | $\Delta_4=-2.65$<br>$\Delta_5=+4.8$, $\Delta_6=-4.5$ |
| C–H bonds | <0.01 | <0.01 |
| C–I bond, atoms 1 and 4 | +0.38 | +0.37 |
| C–Br bond, atoms 1 and 5 | −0.10 | −0.10 |
| H–C–H angle, atoms 2, 1, and 3 | −1.6 | −1.4 |
| H–C–I angle, atoms 2, 1, and 4 | −1.0 | −0.4 |
| H–C–Br angle, atoms 2, 1, and 5 | +6.5 | +6.9 |
| H–C–I angle, atoms 3, 1, and 4 | −1.0 | −0.4 |
| H–C–Br angle, atoms 3, 1, and 5 | +6.5 | +6.9 |
| I–C–Br angle, atoms 4, 1, and 5 | −9.9 | −12 |
| | Range of displacements at $t=15$ fs[a] | |
| B band<br>Internal coordinate | $\Delta_4=+2.5$<br>$\Delta_5=+3.0$, $\Delta_6=+3.6$ | $\Delta_4=+2.5$<br>$\Delta_5=+3.0$, $\Delta_6=-3.6$ |
| C–H bonds | −0.01 | −0.01 |
| C–I bond, atoms 1 and 4 | +0.02 | +0.01 |
| C–Br bond, atoms 1 and 5 | +0.26 | +0.26 |
| H–C–H angle, atoms 2, 1, and 3 | −0.7 | −0.5 |
| H–C–I angle, atoms 2, 1, and 4 | +7.6 | +8.1 |
| H–C–Br angle, atoms 2, 1, and 5 | −2.7 | −2.5 |
| H–C–I angle, atoms 3, 1, and 4 | +7.6 | +8.1 |
| H–C–Br angle, atoms 3, 1, and 5 | −2.7 | −2.5 |
| I–C–Br angle, atoms 4, 1, and 5 | −8.8 | −11 |

[a]Values are for the two most probable sign combinations of the normal mode displacements (see the text).

after photoexcitation in the A band, and these internal coordinate displacements are given in the first part of Table V. Figure 8 shows the geometry of bromoiodomethane with the atoms labeled with numbers and this may be used with Table V to help visualize the short-time photodissociation dynamics.

Choosing the sign combinations that are most probable for the B band is a little more complex. The molecular beam experiments of Lee and co-workers[2,3] showed that photoexcitation at 210 nm results in approximately 59% of the molecules, directly breaking the C–Br bond to form $CH_2I$ and Br, about 35% break both the C–Br and C–I bonds (also apparently in a direct manner) to form $CH_2$+I+Br, and about 6% break both C–I and C–Br bonds to form $CH_2$ and electronically excited IBr. Our deconvolution of the gas phase bromoiodomethane B band shows that the 210 nm absorption has approximately 76% contribution from $^3Q_0$, 18% contribution from $^1Q_1$, and 5% contribution from $^3Q_1$ transitions. From the preceding two sentences, it is tempting to speculate that excitation of the $^3Q_0$ transition corresponds mainly to the $CH_2BrI \rightarrow CH_2I+Br$ channel, excitation of the $^1Q_1$ transition corresponds mostly to the $CH_2BrI \rightarrow CH_2+I+Br$ channel, and excitation of the $^3Q_1$ channel corresponds to the $CH_2BrI \rightarrow CH_2+IBr^*$ channel. However, it is probable that only a $^1Q$ transition could correlate with the $CH_2BrI \rightarrow CH_2+IBr^*$ channel if the electron spin is conserved during the photodissociation. Lee and co-workers[2,3] put forward a LCAO-MO least motion path model with conservation of electron spin for explaining the concerted elimination of electronically excited IBr. In this LCAO-MO model the C–Br bond lengthens and the I–C–Br angle gets smaller so that the $p_z$ orbitals on the Br and I atoms become better aligned and can form the $\sigma$ and $\sigma^*$ orbitals of IBr. Since there are three electrons in the $p_z$ orbitals, the IBr formed will have one of these electrons put into the $\sigma^*$ orbital, and thus the IBr will only be formed electronically excited, and this was consistent with the molecular beam results of Butler, *et al.*[2,3] Therefore, it is most likely that excitation of the $^1Q_1$ transition at 210 nm in gas phase bro-

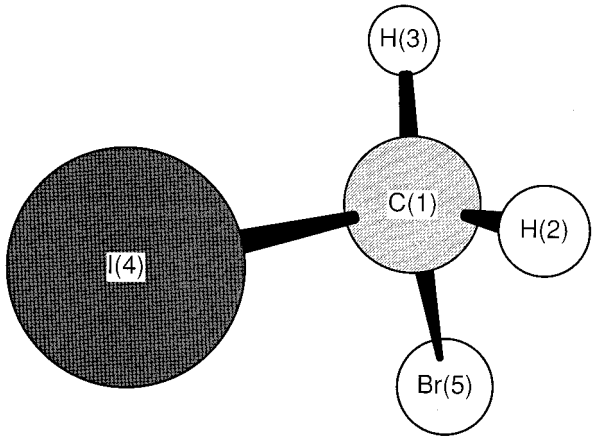


FIG. 8. Geometry of bromoiodomethane with each atom labeled with a number 1 through 5.

moiodomethane will correlate with the $CH_2BrI \rightarrow CH_2 + IBr^*$ channel as well as the $CH_2BrI \rightarrow CH_2 + I + Br$ channel. This would be consistent with both the Gaussian deconvolution of the gas phase absorption spectrum and the molecular beam results. A curve crossing from the $^3Q_0$ to the $^1Q_1$ state could account for the molecules that were initially excited via the $^3Q_0$ transition, but end up in the $CH_2BrI \rightarrow CH_2 + I + Br$ channel, and this would resolve the apparent differences between our deconvolution of the gas phase absorption spectrum and the observed photoproduct branching ratios observed by Lee and co-workers.[2,3] We note that the curve crossing from the $^3Q_0$ to the $^1Q_1$ state is well known for the photodissociation of iodomethane in the A band.[96,97,101–113] However, work done on the A band of bromomethane showed no apparent curve crossing of the $^3Q_0$ and $^1Q_1$ states.[86] Although our deconvolution of the bromoiodomethane absorption spectrum and tentative assignments of the photodissociation channels to the optical transitions suggest the curve crossing of the $^3Q_0$ and $^1Q_1$ states is important for the B-band bromoiodomethane photodissociation channels, we cannot unambiguously determine this and additional experimental data such as MCD measurements are needed to completely resolve this issue.

Now back to choosing the signs of the normal mode displacements for the B band of bromoiodomethane. Since there is predominantly C–Br bond breaking in the B band, one would expect there to be significant lengthening of the C–Br bond, and this implies that the $\Delta_4$ should be positive in sign. Furthermore, since there appears to be some probability of having the C–I bond breaking as well, we could also expect that the C–I bond may also be lengthening as well as the C–Br bond. In order for the C–I bond to lengthen in the Franck–Condon region, the sign of $\Delta_5$ needs to be positive. Thus, the most probable sign combinations of the normal coordinate displacements for the B band of bromoiodomethane appears to be positive for $\Delta_4$, positive for $\Delta_5$, and $\Delta_6$ may be either positive or negative in sign. We note that in both the A-band and B-band photodissociation dynamics of bromoiodomethane, the choice of sign of $\Delta_6$ only changes the magnitude but not the sign of the internal coordinate displacements. The most probable internal coordinate displacements at 15 fs after photoexcitation are given in the last part of Table V.

The A-band photodissociation shows that the C–I bond lengthens significantly ($+0.37$ to $+0.38$ Å), the C–Br bond shortens (about $-0.10$ Å), the I–C–Br angle becomes significantly smaller ($-9.9$ to $-12°$), the H–C–Br angles become larger ($+6.5°$ to $+6.9°$), the H–C–I angles become slightly smaller ($-0.4°$ to $-1.0°$), the H–C–H angle becomes smaller ($-1.4°$ to $1.6°$), and the C–H bonds change very little. These A-band short-time dynamics are consistent with direct C–I bond breaking and the $CH_2Br$ fragment changing toward a more planar structure. The changes in the C–I bond length, the H–C–Br angles, the H–C–I angles, and the I–C–Br angle are all qualitatively consistent with a ''soft'' radical model of the photodissociation dynamics in which the carbon atom is pushed into the rest of the radical fragment. However, the ''soft'' radical model would also predict that the H–C–H angle should become larger instead of smaller. This suggests that the H–C–H angles move toward the planar geometry of the ground state $CH_2Br$ radical at a slower rate than the H–C–Br angles. The ''soft'' radical model in its simplest version assumes that all of the radical fragment atoms are very loosely bound to one another to about the same amount and does not account for the ''stiffness'' of the different bonds (force constants). The C–H stretch and H–C–H bend motions have significantly higher frequencies than motions associated with the C, I, and Br atoms, and it seems that the H–C–H bend and C–H stretch motions are relatively uncoupled from the initial stages of the C–I bond cleavage. It also appears that the higher-frequency H–C–I bend changes slower than the lower-frequency I–C–Br bend during the initial part of the C–I bond dissociation. The A-band photodissociation short-time dynamics seem more consistent with a ''semirigid'' radical model in which C–I bond breaking pushes the carbon atom into a semirigid radical (with appropriate force constants for the radical group) similar to a model suggested by Riley and Wilson.[114]

The B-band bromoiodomethane early-time photodissociation dynamics revealed by Table V shows some similarities as well as some differences with the A-band photodissociation dynamics. Examination of Table V shows that at 15 fs the C–Br bond lengthens substantially ($+0.26$ Å), the C–I bond lengthens slightly ($+0.01$ to $+0.02$ Å), the I–C–Br angle becomes smaller ($-8.8°$ to $-11°$), the H–C–I angles become larger ($+7.6°$ to $8.1°$), and the H–C–Br angles become smaller ($-2.5°$ to $2.7°$). The C–H bonds ($-0.01$ Å) and the H–C–H angle ($-0.5°$ to $-0.7°$) change slightly. The B-band short-time photodissociation dynamics like the A band are more qualitatively consistent with a ''semirigid'' radical model of the photodissociation than a ''soft'' radical model of the photodissociation. However, as the C–I bond breaks in the A band then the C–Br bond becomes shorter, while as the C–Br bond breaks in the B band then the C–I bond becomes longer. In the B band, both the C–Br and C–I bonds are becoming longer, although the C–Br bond lengthens to a much greater extent compared to the C–I bond. As both C–I and C–Br bonds lengthen (weakening the bonds) and the I–C–Br angle becomes smaller, there may be a chance for intramolecular electronic energy transfer so that both the C–I and C–Br bonds break in addition to the predominant C–Br bond breaking associated with the B band of bromoiodomethane.

It is interesting to compare our results for bromoiodomethane with the short-time photodissociation dynamics derived from resonance Raman intensity analysis of iodomethane.[89,90,98,99,115–117] Resonance Raman studies on the A-band absorption of iodomethane have shown that the resonance Raman spectra have a long overtone progression of the nominal C–I stretch mode ($n\nu_3$) and a much smaller progression of combination bands of this mode with the methyl umbrella mode ($\nu_2 + n\nu_3$). This implies that most of the initial A-band photodissociation dynamics involves lengthening of the C–I bond with some methyl umbrella motion occurring as the C–I bond is broken. Our A-band and

B-band short-time photodissociation dynamics are somewhat similar in that as the C–X bond lengthens, the $CH_2Y$ radical moves toward a more planar structure. However, the short-time photodissociation dynamics of bromoiodomethane appears to have more multidimensionality as well as asymmetry than the photodissociation dynamics of A-band iodomethane, which seems close to pseudotriatomic (or even pseudodiatomic) in character. The short-time photodissociation dynamics of bromoiodomethane also appears to have significant changes in both the C–Br and C–I bond lengths, while there is apparently no corresponding change in the C–H bond length in the iodomethane short-time photodissociation dynamics. Several polarization-resolved resonance Raman studies have been performed for the iodomethane A-band absorption in order to investigate the composition of the A-band absorption and the effects of the $^3Q_0 \rightarrow {}^1Q_1$ curve crossing on the resonance Raman spectra.[89,90,98,99,115] A recent study with higher resolution and better signal to noise than previous studies showed that the 266 nm resonance Raman depolarization ratios may arise mainly from simple interference between parallel and perpendicular sources of Raman scattering and curve crossing dynamics appear to have only a small contribution to the resonance Raman spectra.[99] We are currently taking depolarization ratio measurements for bromoiodomethane in solution in order to find out more about the composition of the A-band and B-band absorption spectra, and perhaps the extent of coupling of the C–Br and C–I chromophores, and these results will be reported in the future.[73]

In addition to the extensive and elegant resonance Raman work on the A-band absorption of iodomethane,[89,90,98,99,115–117] there are several in depth and excellent resonance Raman studies on the B band of iodomethane.[118–124] The iodomethane B-state absorption system from 191 to 201 nm is composed of 6*s* Rydberg vibronic transitions that are rotationally diffuse due to very fast predissociation (however, not so fast as to lose vibronic resolution). Therefore the B state is quasibound instead of unbound like the lower lying A state of iodomethane. The B-state Rydberg transitions show a strong origin, a moderate progression in the totally symmetric umbrella bending mode ($\nu_2$), and a few weaker bands corresponding to the C–H stretch ($\nu_1$), the C–I stretch ($\nu_3$), and methyl rock ($\nu_6$) vibrational modes. Careful and extensive Raman polarization and excitation profile measurements[119–121] have found that the B-state origin and the next $\nu_6$ vibronic band have lifetimes of $0.5+/-0.1$ ps (1.2 ps for $CD_3I$). Further studies[122] found vibrationally specific subrotational period lifetimes for several other bands: one quantum of the C–I stretch ($\nu_3$) has a lifetime of ~1.5 ps (~5.0 ps for $CD_3I$), two quantum of the C–I stretch ($2\nu_3$) has a lifetime of ~0.5 ps, and one quantum of the C–H stretch ($\nu_1$) has a lifetime of ~0.06 ps (~0.6 ps for $CD_3I$). The vibrational mode-specific lifetimes (or predissociation rates) were attributed to the multidimensional reaction coordinate in the curve crossing region of B-state and unbound surface.[122] The B-band absorption of bromoiodomethane has no vibronic structure and appears to be an unbound valence transition similar to the A-band absorption of iodomethane or bromomethane. Our B-band bromoiodomethane resonance Raman spectra and inferred short-time photodissociation dynamics are also most consistent with an unbound valence excited state. We do note that the B-band absorption of bromoiodomethane could be influenced by the nearby Rydberg states corresponding to the 6*s* Rydberg transitions of iodomethane. It is possible that the unbound state that predissociates the bound Rydberg transitions in the B state of iodomethane could also cross the nearby B-band transitions of bromoiodomethane and be responsible for the three different dissociation channels associated with the B-band absorption of bromoiodomethane. It would also be quite interesting to compare the 6*s* Rydberg transitions and predissociation dynamics of iodomethane with those found in bromoiodomethane to see the changes induced by the presence of the C–Br chromophore.

There appears to be little quantitative resonance Raman work reported for bromomethane. The A-band absorption of bromomethane is very weak and very close to the Rydberg transitions below 200 nm, so it may be fairly difficult to attribute the resonance Raman intensity solely to A-band transitions without a careful resonance Raman excitation profile to determine possible contributions from other states. However, such a resonance Raman study would be interesting to compare to bromoiodomethane and iodomethane.

Butler *et al.*[2,3] have previously proposed a model for electronic energy transfer to help understand the very different results found for the photodissociation of 1,2-$C_2F_4BrI$ and bromoiodomethane. We will only briefly describe the model and the reader is referred to Refs. 3 and 125 for the more complete and original description. Essentially, as some of the electronic energy goes into the kinetic energy making the C–Br bond longer, there will be some C–Br bond length where the electronic energy of the C–Br bond will equal the energy required to excite the $n \rightarrow \sigma^*$ transition on the C–I bond, with the chance for a near-resonant energy transfer taking place that would give another state that has an electronically excited C–I bond and a vibrationally excited C–Br bond. The intramolecular electronic energy transfer could proceed by an electron exchange and/or a dipole–dipole interaction. The dipole–dipole mechanism is probably more likely, and it could compete with the C–Br bond breaking according to rough calculations carried out by Butler *et al.* for the 1,2-$C_2F_4BrI$ molecule.[3] In the 1,2-$C_2F_4BrI$ molecule the C–I and C–Br chromophores are nearly parallel to one another (which presumably would greatly allow the dipole–dipole interaction electronic energy transfer), while in bromoiodomethane the angle between the C–I and C–Br chromophores is 113° and gets smaller during the initial dissociation (possibly close to 90° near the resonant energy transfer region), which would make the dipole–dipole interaction term much smaller and the near-resonant electronic energy transfer probability would be much smaller in bromoiodomethane. It is quite interesting to note that the $^1Q_1$ transition appears to be correlated with the $CH_2BrI \rightarrow CH_2 + IBr^*$ channel and simultaneous C–I and C–Br bond cleavage, while the $^3Q_0$ transition appears to be primarily correlated with the $CH_2BrI \rightarrow CH_2I + Br$ channel

and cleavage of only the C–Br bond. This brings up the possibility that the near-resonant electronic energy transfer is substantially more efficient for $^1Q$ states than $^3Q$ states and the transfer region occurs where the C–Br bond has enough kinetic energy to go on to break and the electronic energy transferred to the C–I bond gives simultaneous bond cleavage leading to the formation of the $CH_2+I-Br$ channel and the $CH_2+IBr^*$ channel, depending on the relative positions of the I and Br at the time of electronic energy transfer.

We would like to propose a hypothesis for the B-band bromoiodomethane photodissociation. The photoexcitation of bromoiodomethane via the dominant $^3Q_0$ transition (approximately 76% of initially excited molecules at 210 nm according to our deconvolution of the gas phase absorption spectrum) leads predominantly to C–Br bond cleavage (about 59% or slightly less of initially excited molecules at 210 nm according to molecular beam results) and some curve crossing to the $^1Q_1$ surface (about 17% or slightly more of the initially excited molecules at 210 nm). The molecules that are on the $^1Q_1$ surface from either initial photoexcitation (about 18% of initially excited molecules at 210 nm) or curve crossing from the $^3Q_0$ surface (17% or slightly more at 210 nm) proceed to either the $CH_2+I+Br$ channel (about 33%–35% of the initially excited molecules at 210 nm) or the $CH_2+IBr^*$ channel ($<6\%$ of initially excited molecules at 210 nm), depending on the relative positions of the I and Br at the time of electronic energy transfer between the C–Br and C–I chromophores. The $^3Q_1$ transition has such a small percentage of initially excited molecules at 210 nm that we can only speculate that it probably leads to C–Br bond cleavage though other channels cannot be ruled out.

### D. Coupling of the C–I and C–Br chromophores and future prospects for investigating bromoiodomethane

The short-time photodissociation dynamics shown in Table V for the A band and B band of bromoiodomethane suggests that their is a small amount of coupling of the C–I and C–Br $n\rightarrow\sigma^*$ transitions, since both the C–Br and C–I bonds change in the Franck–Condon of each of the A and B bands. Our simulations of the A-band and B-band resonance Raman intensities and $^3Q_0$ transitions of the absorption spectra assumed that the transitions were completely uncoupled and each transition was modeled separately. While our simulations appear to do a somewhat reasonable job of simulating the major features of the A-band and B-band resonance Raman intensities and absorption spectra, there are several wavelength-dependent trends in the resonance Raman intensities that we are unable to model using uncoupled transitions. For example, in the B-band resonance Raman spectra the $2\nu_4$, $2\nu_4+\nu_5$, and $2\nu_4+2\nu_5$ relative intensities increase greatly as the excitation energy increases. This may indicate that the C–Br character of the transition becomes greater as the excitation energy increases. Similarly, the A-band transitions of $3\nu_5$, $4\nu_5$, and $\nu_4+3\nu_5$ increase fairly strongly as the excitation energy decreases. This could indicate that the C–I character of the A band increases as the excitation energy decreases. We plan to develop a model in the future that includes coupling of the dominant A-band and B-band transitions in order to examine the effect of coupling of the C–I and C–Br chromophores on the resonance Raman intensities, and this may substantially improve the agreement between the simulations and the resonance Raman experimental intensities. We also plan to carry out additional resonance Raman experiments including depolarization ratio measurements in the future to explore solvent effects on the short-time photodissociation dynamics of bromoiodomethane. These experiments would explore the possibility of solvent-induced and/or solvent-dependent mixing of electronic states, as well as the solvent dependence of bond selective photochemistry. Comparison of the absorption spectra of bromoiodomethane in the gas phase and in cyclohexane solution shown in Fig. 1 shows that there appears to be significant changes in the relative positions and intensities of the electronic transitions upon solvation, particularly for the B-band transitions. This suggests that there may be noticeable solvation and solvent-dependent effects on the mixing of electronic states and/or bond selective photodissociation dynamics and photochemistry. Bromoiodomethane has the opportunity to examine the electronic mixing and bond selective photochemistry in a wide range of molecular environments ranging from the gas phase (isolated molecules) to condensed phase nonpolar solvents, and even polar solvents such as methanol and acetonitrile.

In contrast to iodomethane, bromoiodomethane has not been nearly as extensively studied, either experimentally or theoretically. This is somewhat surprising since bromoiodomethane has a very similar structure, and the same number of atoms as iodomethane and bromoiodomethane can be considered one of the prototypes for bond selective electronic excitation and photochemistry. Bromoiodomethane also has many facets of its photodissociation and its electronic states in the A and B bands that would be very interesting to understand in more detail. For example, wavelength-dependent studies of the B band can help reveal the wavelength dependence of the three different photodissociation channels quantum yields, explore how important a $^3Q_0$ curve crossing to the $^1Q_1$ state (or possibly others) may be, and shed more light on the mechanism that breaks both the C–I and C–Br (presumably simultaneously) in the two minor dissociation channels. It would also be very intriguing to further elucidate the mechanism and sources of the absorption intensity enhancement and redshifts of the A and B bands of bromoiodomethane relative to the single chromophore iodomethane and bromomethane molecules. Many of the experimental techniques such as molecular beam experiments,[101–105,107] magnetic circular dichroism (MCD),[85] multiphoton ionization (MPI),[107,126–128] infrared emission,[106] coherent anti-Stokes Raman scattering (CARS),[129] diode laser absorption,[130] femtosecond time-resolved pump-probe experiments,[95] and others that have proved so useful to study iodomethane A-band photodissociation are readily applicable to the bromoiodomethane system. The bromoiodomethane molecular system appears ripe for a wide variety of experimental and possibly theoretical work by many different research groups to help create a much more detailed under-

standing of its bond selective electronic excitation and photochemistry.

## V. CONCLUSION

We have presented resonance Raman spectra and absolute Raman cross section measurements of bromoiodomethane in cyclohexane solution taken with eight excitations in the spectral region of the A-band and B-band absorptions. We have used a relatively simple model to calculate the resonance Raman intensities and absorption bands. The results of these time-dependent wave packet calculations were used in conjunction with the normal mode vibrational descriptions to obtain the short-time photodissociation dynamics in terms of easy to visualize internal coordinate changes. The short-time photodissociation dynamics ($\sim$15 fs) associated with the dominant $^3Q_0$ transition of the A band of bromoiodomethane shows that the C–I bond becomes substantially longer, the C–Br bond becomes somewhat shorter, the I–C–Br angle becomes smaller, the H–C–Br angles become larger, the H–C–I angles and the H–C–H angle become slightly smaller, and the C–H bonds do not change much. The dominant $^3Q_0$ transition with the B-band absorption of bromoiodomethane has the following early-time ($\sim$15 fs) photodissociation dynamics: the C–I bond becomes only slightly longer, the C–Br bond becomes substantially longer, the I–C–Br angle becomes smaller, the H–C–Br angles become smaller, the H–C–I angles become larger, the H–C–H angle become slightly smaller, and the C–H bonds do not change much. The photodissociation dynamics of bromoiodomethane associated with both the A band and B bands seem most consistent with an impulsive ''semirigid'' radical model qualitative description with the $CH_2Br$ radical moving toward a more planar structure in the A band and the $CH_2I$ radical moving toward a more planar structure in the B band.

We have also presented Gaussian deconvolutions of the absorption spectra of bromoiodomethane in cyclohexane solution, gas phase bromoiodomethane, gas phase iodomethane, and gas phase bromomethane in order to estimate the relative contributions of the different $n\rightarrow\sigma^*$ transitions to the absorption bands. Comparison of the Gaussian deconvolution of bromoiodomethane with the single chromophore iodomethane and bromomethane deconvolutions shows that the $^3Q_0$ transitions appear to be enhanced to a significantly greater extent than the $^3Q_1$ and $^1Q_1$ transitions, and the enhancement of the B-band transitions are greater than the A-band transitions relative to their respective single chromophore transitions. The patterns in the Gaussian deconvolutions, the resonance Raman intensities, and the short-time photodissociation dynamics of the A band and B bands all suggest a moderate degree of coupling between the C–I and C–Br chromophores. We have also presented a simple speculative description of the B-band photodissociation that is consistent with our Gaussian deconvolution of the absorption spectrum and possibly the previous results of molecular beam experiments reported by Butler *et al.*[3]

## ACKNOWLEDGMENTS

This work was supported by grants from the Committee on Research and Conference Grants (CRCG), the Research Grants Council (RGC) of Hong Kong, the Hung Hing Ying Physical Sciences Research Fund, and the Large Items of Equipment Allocation 1993–94 from the University of Hong Kong.

[1] S. J. Lee and R. Bersohn, J. Phys. Chem. **86**, 728 (1982).
[2] L. J. Butler, E. J. Hintsa, and Y. T. Lee, J. Chem. Phys. **84**, 4104 (1986).
[3] L. J. Butler *et al.*, J. Chem. Phys. **86**, 2051 (1987).
[4] L. Zhang, W. Fuss, and K. L. Kompa, Chem. Phys. **144**, 289 (1990).
[5] F. F. Crim, Annu. Rev. Phys. Chem. **44**, 397 (1993).
[6] L. J. Butler *et al.*, J. Chem. Phys. **85**, 2331 (1986).
[7] T. M. Tichich *et al.*, J. Chem. Phys. **87**, 5820 (1987).
[8] R. L. Vander Wal, J. L. Scott, and F. F. Crim, J. Chem. Phys. **92**, 803 (1990).
[9] R. L. Vander Wal *et al.*, J. Chem. Phys. **94**, 3548 (1991).
[10] N. Shafer, S. Satyapal, and R. Bersohn, J. Chem. Phys. **90**, 6807 (1989).
[11] S. Satyapal and R. Bersohn, J. Phys. Chem. **95**, 8004 (1991).
[12] M. D. Person *et al.*, J. Chem. Phys. **95**, 3843 (1991).
[13] J. S. Keller *et al.*, J. Chem. Phys. **96**, 4324 (1992).
[14] M. D. Person, P. W. Kash, and L. J. Butler, J. Chem. Phys. **97**, 355 (1992).
[15] P. W. Kash, G. C. G. Waschewsky, and L. J. Butler, J. Chem. Phys. **99**, 4479 (1993).
[16] P. W. Kash *et al.*, J. Chem. Phys. **99**, 4479 (1993).
[17] G. C. G. Waschewsky *et al.*, J. Chem. Soc. Faraday Trans. **90**, 1581 (1994).
[18] P. Andresen *et al.*, J. Chem. Phys. **83**, 1429 (1985).
[19] I. Bar *et al.*, J. Chem. Phys. **95**, 3341 (1991).
[20] M. Brouard *et al.*, Mol. Phys. **69**, 65 (1990).
[21] P. R. Fleming, M. Li, and T. R. Rizzo, J. Chem. Phys. **95**, 865 (1991).
[22] P. F. Zittel and V. I. Lang, J. Photochem. Photobiol. A **56**, 149 (1991).
[23] S. M. Holland *et al.*, J. Chem. Soc. Faraday Trans. **87**, 3461 (1991).
[24] K. Tonokura *et al.*, J. Chem. Phys. **95**, 5065 (1991).
[25] K. Seki and H. Okabe, J. Phys. Chem. **96**, 3345 (1992).
[26] J. L. Brum *et al.*, J. Chem. Phys. **98**, 1178 (1993).
[27] M. Shapiro, J. W. Hepburn, and P. Brumer, Chem. Phys. Lett. **149**, 451 (1988).
[28] P. Brumer and M. Shapiro, Acc. Chem. Res. **22**, 407 (1989).
[29] T. Seideman, M. Shapiro, and P. Brumer, J. Chem. Phys. **90**, 7132 (1989).
[30] I. Levy, M. Shapiro, and P. Brumer, J. Chem. Phys. **93**, 2493 (1990).
[31] M. Shapiro and P. Brumer, J. Chem. Phys. **95**, 8658 (1991).
[32] M. Shapiro and P. Brumer, Annu. Rev. Phys. Chem. **43**, 257 (1992).
[33] Z. Chen, M. Shapiro, and P. Brumer, J. Chem. Phys. **102**, 5683 (1995).
[34] D. J. Tannor and S. A. Rice, J. Chem. Phys. **83**, 5013 (1985).
[35] D. J. Tannor, R. Kosloff, and S. A. Rice, J. Chem. Phys. **85**, 5805 (1986).
[36] D. J. Tannor and S. A. Rice, Adv. Chem. Phys. **70**, 441 (1988).
[37] R. Kosloff *et al.*, Chem. Phys. **139**, 201 (1989).
[38] S. Shi, A. Woody, and H. Rabitz, J. Chem. Phys. **88**, 6870 (1988).
[39] S. Shi and H. Rabitz, Chem. Phys. **139**, 185 (1989).
[40] R. S. Judson *et al.*, J. Mol. Struct. **223**, 425 (1990).
[41] S. Chelkowski, A. Bandrauk, and P. B. Corkum, Phys. Rev. Lett. **65**, 2355 (1990).
[42] C. Chen, Y.-Y. Yin, and D. S. Elliot, Phys. Rev. Lett. **64**, 507 (1990).
[43] S. M. Park, S.-P. Lu, and R. J. Gordon, J. Chem. Phys. **94**, 8622 (1991).
[44] B. A. Baranova, A. N. Chudinov, and B. Ya. Zel'dovitch, Opt. Commun. **79**, 116 (1990).
[45] S.-P. Lu *et al.*, J. Chem. Phys. **96**, 6613 (1992).
[46] P. A. Schulz *et al.*, Annu. Rev. Phys. Chem. **30**, 379 (1979), and references therein.
[47] F. F. Crim, Annu. Rev. Phys. Chem. **35**, 657 (1984), and references therein.
[48] T. Uzer, Phys. Rep. **199**, 73 (1991), and references therein.
[49] A. Sinha, M. C. Hsiao, and F. F. Crim, J. Chem. Phys. **92**, 6333 (1990).
[50] A. Sinha, M. C. Hsiao, and F. F. Crim, J. Chem. Phys. **94**, 4928 (1991).
[51] M. J. Bronikowski *et al.*, J. Chem. Phys. **95**, 8647 (1991).
[52] M. J. Bronikowski, W. R. Simpson, and R. N. Zare, J. Chem. Phys. **97**, 2194 (1993).

[53] M. J. Bronikowski, W. R. Simpson, and R. N. Zare, J. Chem. Phys. **97**, 2204 (1993).
[54] A. Sinha, J. D. Thoemke, and F. F. Crim, J. Chem. Phys. **96**, 372 (1992).
[55] R. B. Metz *et al.*, J. Chem. Phys. **99**, 1744 (1993).
[56] Y.-F. Yen *et al.*, J. Phys. Chem. **98**, 4 (1994).
[57] W. M. Kwok and D. L. Phillips, Chem. Phys. Lett. **235**, 260 (1995).
[58] W. M. Kwok and D. L. Phillips, J. Chem. Phys. **104**, 2529 (1996).
[59] A. E. Johnson and A. B. Myers, J. Chem. Phys. **102**, 3519 (1995).
[60] A. E. Johnson and A. B. Myers, J. Phys. Chem. (in press).
[61] U. Banin, R. Kosloff, and S. Ruhman, Isr. J. Chem. **33**, 141 (1993).
[62] S. Ruhman (private communication).
[63] J. Zhang and D. G. Imre, J. Chem. Phys. **89**, 309 (1988).
[64] J. Zhang *et al.*, J. Chem. Phys. **89**, 3602 (1988).
[65] S. Miyano and H. Hashimoto, Bull. Chem. Soc. Jpn. **44**, 2864 (1971).
[66] D. L. Phillips and W. M. Kwok, Chem. Phys. Lett. **241**, 267 (1995).
[67] S.-Q. Man, W. M. Kwok, and D. L. Phillips, J. Phys. Chem. **99**, 15705 (1995).
[68] W. M. Kwok and D. L. Phillips, J. Chem. Phys. (in press).
[69] A. B. Myers, B. Li, and X. Ci, J. Chem. Phys. **89**, 1876 (1988).
[70] A. B. Myers, in *Laser Techniques in Chemistry*, edited by A. B. Myers and T. R. Rizzo (Wiley, New York, 1995), p. 325.
[71] M. O. Trulson and R. A. Mathies, J. Chem. Phys. **84**, 2068 (1986).
[72] B. Li and A. B. Myers, J. Phys. Chem. **94**, 4051 (1990).
[73] S.-Q. Man, W. M. Kwok, and D. L. Phillips (unpublished).
[74] S. Y. Lee and E. J. Heller, J. Chem. Phys. **71**, 4777 (1979).
[75] E. J. Heller, Acc. Chem. Res. **14**, 368 (1981).
[76] E. J. Heller, R. J. Sundberg, and D. Tannor, J. Phys. Chem. **86**, 1822 (1982).
[77] A. B. Myers *et al.*, J. Chem. Phys. **77**, 3857 (1982).
[78] J. Sue, Y. J. Yan, and S. Mukamel, J. Chem. Phys. **85**, 462 (1986).
[79] Y. J. Yan and S. Mukamel, J. Chem. Phys. **86**, 6085 (1987).
[80] B. U. Curry, Ph.D. dissertation, University of California, Berkeley, 1983.
[81] M. Z. El-Sabban, A. Danti, and B. J. Zwolinski, J. Chem. Phys. **44**, 1770 (1966).
[82] W. Bacher and J. Wagner, Z. Phys. Chem. B **43**, 191 (1939).
[83] J. Wagner, Z. Phys. Chem. B **45**, 69 (1939).
[84] See AIP Document No. PAPS JCPSA-105-5842-7 for 7 pages of tables. Order by PAPS number and journal reference from American Institute of Physics, Physics Auxiliary Publication Service, Carolyn Gehlbach, 500 Sunnyside Boulevard, Woodbury, New York 11797-2999. Fax: 516-576-2223; e-mail: paps@aip.org. The price is $1.50 for each microfiche (98 pages) or $5.00 for photocopies of up to 30 pages, and $0.15 for each additional page over 30 pages. Airmail additional. Make checks payable to the American Institute of Physics.
[85] A. Gedanken and M. D. Rowe, Chem. Phys. Lett. **34**, 39 (1975).
[86] G. N. A. Van Veen, T. Baller, and A. E. DeVries, Chem. Phys. **92**, 59 (1985).
[87] M. B. Robin, Can. J. Chem. **63**, 2032 (1985).
[88] D. L. Phillips and A. B. Myers, J. Chem. Phys. **95**, 226 (1991).
[89] G. E. Galica *et al.*, J. Phys. Chem. **95**, 7994 (1991).
[90] F. Markel and A. B. Myers, J. Chem. Phys. **98**, 21 (1993).
[91] X. Ci and A. B. Myers, J. Chem. Phys. **96**, 6433 (1992).
[92] A. B. Myers and K. S. Pranata, J. Phys. Chem. **93**, 5079 (1989).
[93] X. Ci, M. A. Pereira, and A. B. Myers, J. Chem. Phys. **92**, 4708 (1990).
[94] B. J. Schwartz *et al.*, Chem. Phys. Lett. **203**, 503 (1993).
[95] L. R. Khundar and A. H. Zewail, Chem. Phys. Lett. **142**, 426 (1987).
[96] H. Guo and G. C. Schatz, J. Chem. Phys. **95**, 3091 (1991).
[97] H. Guo, J. Chem. Phys. **96**, 2731 (1992).
[98] K. Q. Lao *et al.*, J. Chem. Phys. **92**, 823 (1990).
[99] P. G. Wang and L. D. Ziegler, J. Phys. Chem. **97**, 3139 (1993).
[100] A. B. Myers and R. A. Mathies, in *Biological Applications of Raman Spectroscopy*, edited by T. G. Spiro (Wiley, New York, 1987), Vol. 2, p. 1.
[101] M. Dzvonik, S. Yang, and R. Bersohn, J. Chem. Phys. **61**, 4408 (1974).
[102] J. F. Black and I. Powis, Chem. Phys. **125**, 375 (1988).
[103] R. K. Sparks *et al.*, J. Chem. Phys. **75**, 3838 (1981).
[104] G. N. A. Van Veen *et al.*, Chem. Phys. **87**, 405 (1984).
[105] P. Brewer *et al.*, J. Chem. Phys. **79**, 720 (1983).
[106] W. P. Hess *et al.*, J. Chem. Phys. **84**, 2143 (1986).
[107] Q. Zhu *et al.*, Chem. Phys. Lett. **144**, 486 (1988).
[108] M. Shapiro and R. Bersohn, J. Chem. Phys. **72**, 3810 (1980).
[109] S. K. Gray and M. S. Child, Mol. Phys. **51**, 189 (1984).
[110] M. Shapiro, J. Phys. Chem. **90**, 3644 (1986).
[111] M. Tadjeddine, J. P. Flament, and C. Teichteil, Chem. Phys. **118**, 45 (1987).
[112] H. Guo and G. C. Schatz, J. Chem. Phys. **93**, 393 (1990).
[113] Y. Amatsu, K. Morokuma, and S. Yabushita, J. Chem. Phys. **94**, 4858 (1991).
[114] S. J. Riley and K. R. Wilson, Faraday Discuss. Chem. Soc. **53**, 132 (1972).
[115] D. Imre *et al.*, J. Phys. Chem. **88**, 3956 (1984).
[116] M. O. Hale *et al.*, J. Phys. Chem. **90**, 4997 (1986).
[117] M. R. Wedlock *et al.*, J. Phys. Chem. **95**, 8096 (1991).
[118] Y. C. Chung and L. D. Ziegler, J. Chem. Phys. **88**, 7287 (1988).
[119] L. D. Ziegler *et al.*, J. Chem. Phys. **90**, 4125 (1989).
[120] P. G. Wang *et al.*, J. Chem. Phys. **92**, 2806 (1990).
[121] L. D. Ziegler *et al.*, J. Phys. Chem. **94**, 3394 (1990).
[122] P. G. Wang and L. D. Ziegler, J. Chem. Phys. **95**, 288 (1991).
[123] L. D. Ziegler, Acc. Chem. Res. **27**, 1 (1993).
[124] T. Kalbfleisch *et al.*, J. Chem. Phys. **103**, 7673 (1995).
[125] D. Krajnovich, L. J. Butler, and Y. T. Lee, J. Chem. Phys. **81**, 3031 (1984).
[126] I. Powis and J. F. Black, J. Phys. Chem. **93**, 2461 (1989).
[127] R. Ogorzalek-Loo *et al.*, J. Chem. Phys. **90**, 4222 (1989).
[128] D. W. Chandler *et al.*, J. Phys. Chem. **94**, 4839 (1990).
[129] N. E. Triggs *et al.*, J. Chem. Phys. **96**, 1822 (1992).
[130] G. E. Hall, T. J. Sears, and J. M. Frye, J. Chem. Phys. **89**, 580 (1988).